Commun Nonlinear Sci Numer Simulat 39 (2016) 99–107

Contents lists available at ScienceDirect

Commun Nonlinear Sci Numer Simulat

journal homepage: www.elsevier.com/locate/cnsns

The effect of process delay on dynamical behaviors in a self-feedback nonlinear oscillator

Chenggui Yao[a,*], Jun Ma[b], Chuan Li[c], Zhiwei He[a]

[a] Department of Mathematics, Shaoxing University, Shaoxing, China
[b] Department of Physics, Lanzhou University of Technology, Lanzhou, China
[c] Jiangxi Expressway networking management center, Nanchang, China

ARTICLE INFO

Article history:
Received 29 August 2015
Revised 20 December 2015
Accepted 28 February 2016
Available online 4 March 2016

Keywords:
Feedback loop
Process delay
Transmission delay
Amplitude death
Nonlinear oscillator

ABSTRACT

The delayed feedback loops play a crucial role in the stability of dynamical systems. The effect of process delay in feedback is studied numerically and theoretically in the delayed feedback nonlinear systems including the neural model, periodic system and chaotic oscillator. The process delay is of key importance in determining the evolution of systems, and the rich dynamical phenomena are observed. By introducing a process delay, we find that it can induce bursting electric activities in the neural model. We demonstrate that this novel regime of amplitude death also exists in the parameter space of feedback strength and process delay for the periodic system and chaotic oscillator. Our results extend the effect of process delay in the paper of Zou et al.(2013) where the process delay can eliminate the amplitude death of the coupled nonlinear systems.

1. Introduction

The self-feedback loops, connecting a system to itself, are pervasive and significant in many science and application fields [1–4], especially in the biological system [5–7]. Many systems perceive external input in the form of self-feedback circuits, or loops. One of the well studied examples is the autapse which has been named originally by Van et al. in 1972 [8]. The autapses, formed between a neuron and a branch of its own axon, are relatively widespread and have been found in the various brain areas, including the cerebellum, striatum, hippocampus, and neocortex [9,10]. So far, several studies have also revealed that these autapses could play an important role in brain function, maintaining the precision of action potential firing trains. Bekkers revealed that excitatory autapses contribute to a positive-feedback loop that maintains persistent electrical activity in neurons, and the functional autapses in the cerebral cortex are found [11]. Saada et. al have identified an autapse which underlies a plateau potential causing persistent activity in the B31/B32 neurons of Aplysia. The persistent activity is essential to the ability of these neurons to initiate and maintain components of feeding behavior [12]. Bacci et al experimentally observed that firing precision of spike times of neurons was increased in pyramidal neurons by artificial GABAergic autaptic conductances [13], and found that the autaptic activity has significant inhibitory effects on repetitive firing and increase the current threshold for evoking action potentials [14]. Furthermore, the effect of autaptic on neural dynamics is also investigated widely, and many interesting phenomena are observed [15–22].

* Corresponding author. Tel.: +86 15967555901.
E-mail address: yaochenggui2006@126.com (C. Yao).

http://dx.doi.org/10.1016/j.cnsns.2016.02.025
1007-5704/

The time delayed feedback, a particularly simple and efficient scheme, has a significant effect on the dynamics of nonlinear systems, especially on stabilizing periodic orbits and steady states embedded in chaotic attractors in physics, chemistry, biology, and medicine [23–25]. For example, Many works have shown that time-delayed feedback methods provide a tool to stabilize unstable steady states [26–29]. Ahlborn and Parlitz found that the multiple delayed feedback signals can stabilize plane waves or the trapping spiral waves in the two-dimensional complex Ginzburg–Landau equation [30]. Gaudreault et al found that the delay feedback can modify the natural frequency of the oscillator and the damping coefficient [31]. Yanchuk presented an asymptotic analysis of time-delayed feedback control of steady states for large delay time, and elaborated analytical conditions for successful control of a fixed point of focus type [32]. The feedback method has also been applied successfully in many experiments, including laser [33], electronic [34], chemical [35], and plasma systems [36].

The time-delayed feedback, used the difference $g(x(t-\tau))-g(x(t))$, was first introduced by Pyragas [37]. Here, the delay τ is known as the time delay which arises from finite propagation speeds. It has been named as propagation delay which has also been widely investigated, and various phenomena have been uncovered in time-delayed coupling oscillators [38–45]. Very recently, the marked effects of the process delay on dynamical behavior have been revealed [46–49]. The process delay, different with the propagation delay, comes from a finite response time required for internal processing of the input information. The process delay is universal in a heterogeneous network especially in networks with large hubs due to nodes with different time scale of oscillations. In cognitive psychophysiology and cognitive neuroscience, the mental chronometry is a core paradigm of process delay which the neural system deal with the reaction time to a stimulus [50]. Importantly, the experimental evidence of process delay in annihilating the quenching of oscillation will be reported [51]. So far, to the best of our knowledge, in all existing works on the feedback, the effect of process delay on the dynamical behavior of nonlinear systems was not considered.

In this work, we investigate numerically and theoretically the effect of process delay in self-feedback on dynamics of the nonlinear systems including the neural model, periodic system and chaotic oscillator. We show that the rich dynamical phenomena are observed with the different values of feedback strength, propagation delay, and process delay. For the delayed feedback excitable FitzHugh–Nagumo neural model, the propagation delay can induce simply spiking without process delay. Surprisingly, we find that the process delay can drive the neuron to bursting electric activities. For the periodic system and chaotic oscillator, We find that the process delay can stabilize unstable fixed points before the transmission delay takes no effect in stabilization, and the analytical boundaries are also derived explicitly. This paper is organized as follows. In Section 2, we investigate the FitzHugh–Nagumo neuronal model with delay feedback. In Section 3, the case of the Stuart-Landau system is discussed in details. In Section 4, we examine the dynamical behavior of the delayed feedback Rössler oscillator. Finally, Section 5 is devoted to our conclusions and discussions.

2. The FitzHugh–Nagumo neuronal Model

First let us consider the delayed-feedback FitzHugh–Nagumo neuronal model which is described by

$$\epsilon\dot{x} = x - \frac{x^3}{3} - y + I_{syn}, \tag{1a}$$

$$\dot{y} = x + a. \tag{1b}$$

In a neural context, x is the activator variable (representing the membrane potential) and y is the inhibitor (related to the conductivity of the potassium channels existing in the neuron membrane) [52–55]. The dynamics of y is much faster than that of x because of the small parameter $\epsilon = 0.01$. When $|a| < 1$, the unit is in the oscillatory regime, while for $|a| > 1$, it is in the excitable one [54,55]. In our paper, $a = 1.05$ is chosen and fixed [54,56,57]. The decision about choosing parameter a since $a = 1.05$ is near bifurcation point. The more richer dynamical behaviors may be observed for this chosen parameter. I_{syn} is the synaptic current through self-feedback,

$$I_{syn} = \kappa(x(t-\tau-\delta) - x(t-\delta)), \tag{2}$$

where the delays δ and τ physically account for the process time and propagation time, respectively. κ quantifies gain of feedback.

For an electrical autapse with the process delay, the rich firing patterns for the FitzHugh–Nagumo neuronal model are observed. The time series of the action potential for the different autaptic parameters are shown in Fig. 1. In Fig. 1(a) and (b), the autaptic intensity is given as $\kappa = 0.2$, and the process delay time is given as $\delta = 0.8$. Fig. 1(c) and (d), the autaptic intensity is given as $\kappa = 0.4$, and the process delay time is given as $\delta = 0.2$. The FitzHugh–Nagumo neuronal model is on quiescent state for this parameter settings, but it transitions to the various spiking patterns in the presence of an process delay. Fig. 1(a) exhibits a period-1 spiking pattern, Fig. 1(b) give a period-2 spiking pattern, while Fig. 1(c) and (d) are devoted to examples of period-4 and period-7 busting pattern.

To display clearly the effect of process delay in the autapse on the firing patterns, we show the bifurcations of the interspike intervals (ISIs) against propagation delay τ with different process delay δ and the gain of feedback κ, respectively. The neuronal model is in the periodic oscillatory mode without process delay for the sufficiently large τ [Fig. 2(a)]. Comparing three subfigures, the marked effect of the process delay in autaptic is observed [Fig. 2(b) and (c)]. The neuron transmits from

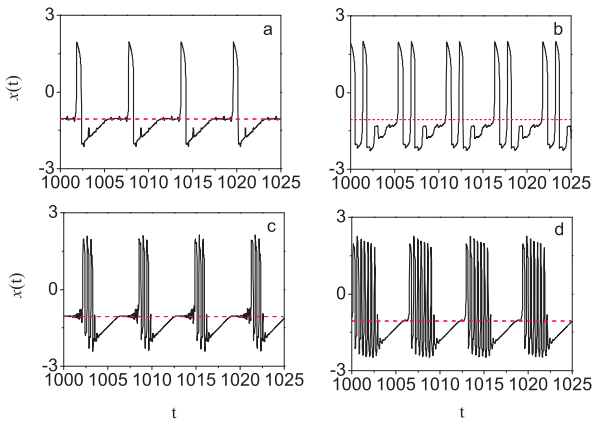

Fig. 1. The time series of $x(t)$ (a) of a period-1 spiking with $\kappa = 0.2, \delta = 0.8, \tau = 0.1$ (b) of a period-2 spiking with $\kappa = 0.2, \delta = 0.8, \tau = 0.5$ (c) of period-4 bursting with $\kappa = 0.4, \delta = 0.2, \tau = 0.05$ and (d) and period-7 busting with $\kappa = 0.4, \delta = 0.2, \tau = 0.1$. The pink dashed lines are the time series of the action potential without the process delay. (For interpretation of the references to color in this figure legend, the reader is referred to the web version of this article).

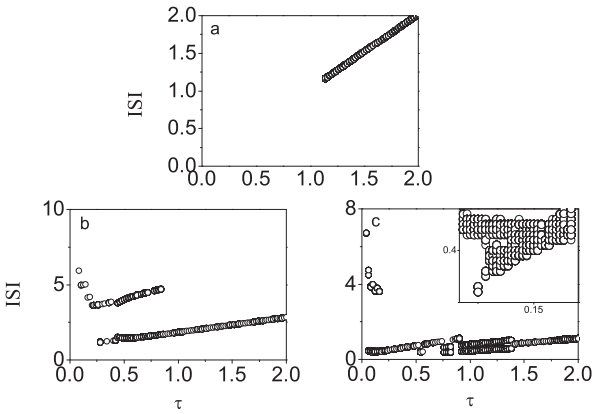

Fig. 2. (a)–(c) The bifurcation diagrams of Δt_i (the interval time of successive spikes) of $x(t)$ for $\kappa = 0.4, \delta = 0$, $\kappa = 0.2, \delta = 0.8$ and $\kappa = 0.4, \delta = 0.2$, respectively. The inset of (c) shows the zoomed-in part of (c), indicating that the bursting electric activity occurs.

quiescent state to regular spiking patterns (period-1 firing pattern) under the action of process delay when the propagation delay is small, then the neuron will undergo bursting patterns as the propagation delay time increases.

To get a global view, the phase diagrams on the plane (δ, τ) are shown numerically in Fig. 3 for the different dynamic regions with $\kappa = 0.2$, and 0.4, respectively. The system behaves five primary features: quiescent state (QS), excite-spiking state(ESS), bursting state (BS), unexcite-oscillate state (UOS), and multistable state (MS). The pink region where a sufficiently large stimulus can excite a spike at the time interval between two successive firing corresponds to ESS; while the green region where any stimulus cannot excite a spike at the time interval between two successive firing corresponds to UOS; the blue region where periods of rapid action potential spiking are followed by a phase quiescent periods corresponds to BS. The multistable region is marked with the orange region. To distinguish the chaotic state and period state, we count Δt_i (the interval time of successive spikes) in a sufficiently large time, if Δt_i's are random, we believe that the system is chaotic. Otherwise, the system is period.

3. The Stuart-Landau oscillator

Next, let us consider the following self-feedback coupled Stuart-Landau oscillator [58]:

$$\dot{z} = (1 + i\omega - |z|^2)z + \kappa(z(t - \tau - \delta) - z(t - \delta)), \tag{3}$$

where $z = x + iy$ represents the complex variable of the oscillator; κ quantifies gain of feedback, and the delays δ and τ physically account for the process time and propagation time, respectively. The ω is the rotational frequency of the limit cycle oscillator. In the absence of feedback (i.e., $\kappa = 0$), the oscillator performs the limit-cycle motion $z = e^{i\omega t}$. When $\kappa > 0$, the occurrence of amplitude death implies the conversion of stability of the fixed point by self-feedback. To identify an amplitude death state, the self-feedback coupled system (3) is linearized at the origin ($z = 0$). The linearization equation of

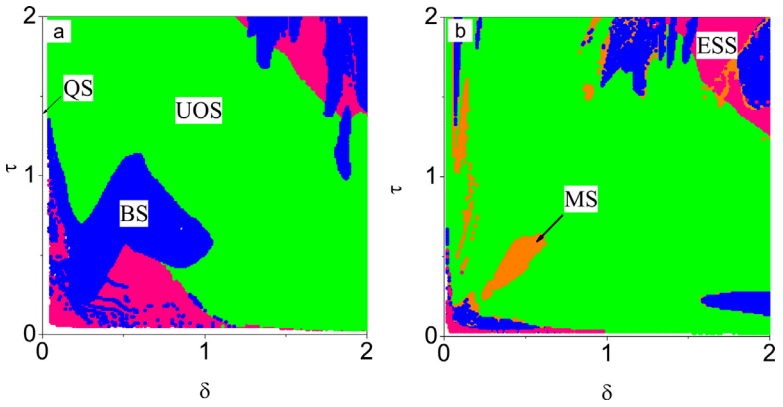

Fig. 3. (a) and (b) Schematic phase diagrams for Eq. (1) in the (δ, τ) plane for different dynamic parameter region with $\kappa = 0.2$ and $\kappa = 0.4$, respectively. The pink region where a sufficiently large stimulus can excite a spike at the time interval between two successive firing corresponds to ESS; while the green region where any stimulus cannot excite a spike at the time interval between two successive firing corresponds to UOS; the blue region corresponds to BS (bursting state) and the multistable region is marked with the orange region. The letter QS stands for the quiescent state. (For interpretation of the references to color in this figure legend, the reader is referred to the web version of this article).

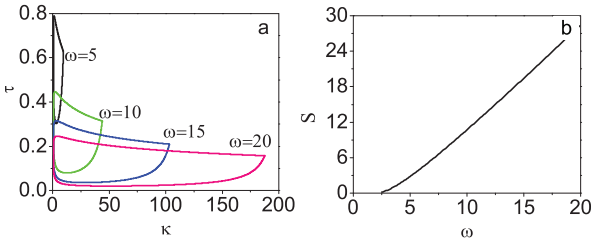

Fig. 4. (a) The amplitude death islands of the self-feedback coupled Stuart-Landau oscillator without process delay for different frequencies. (b) The size of amplitude death region S is plotted against ω.

the amplitude death state reads as:

$$\dot{\xi} = (1 \pm i\omega)\xi + \kappa(\xi(t-\delta-\tau) - \xi(t-\delta)). \tag{4}$$

The characteristic equation for the amplitude death state is obtained by making $\xi \propto e^{\lambda t}$,

$$\lambda = (1 \pm i\omega) + \kappa(e^{-\lambda(\delta+\tau)} - e^{-\lambda\delta}). \tag{5}$$

Setting $\lambda = \alpha + i\beta$, where α and β are real, the amplitude death region corresponds to the region in which $\alpha < 0$. The marginal stability curves or the critical curves are thus obtained by requiring that $\alpha = 0$, i.e. $\lambda = i\beta$. Substituting this in Eq. (5), the equation defining the critical curves is thus given by

$$i\beta = (1 \pm i\omega) + \kappa(e^{-i\beta(\delta+\tau)} - e^{-i\beta\delta}), \tag{6}$$

For $\delta = 0$, we get the critical coupling strength $\kappa_c = 1.0$ and the following bounding curves for the death island region by eliminating β in Eq. (6):

$$\begin{aligned} \tau_a &= \frac{2m\pi + \cos^{-1}\left(\frac{\kappa-1}{\kappa}\right)}{w_0 - \kappa\sqrt{1-\left(\frac{\kappa-1}{\kappa}\right)^2}}, \\ \tau_b &= \frac{2(m+1)\pi - \cos^{-1}\left(\frac{\kappa-1}{\kappa}\right)}{w_0 + \kappa\sqrt{1-\left(\frac{\kappa-1}{\kappa}\right)^2}}, \end{aligned} \tag{7}$$

where m $(m = 0, 1, 2, ..., \infty)$ stands for the number of death islands. These critical curves are similar with the result in paper [28]. The figures for amplitude death surrounded by the above critical curves are shown in Fig. 4 for different frequencies, respectively. One can observe clearly that the size of region of amplitude death monotonically increases as frequency ω increases.

Next, we consider $\delta \neq 0$. The accurate solution may be not gotten for $\delta \neq 0$ due to complexity of Eq. (6), however, we can obtain the approximate solution under the condition $\tau \ll \delta$,

$$i\beta = (1 \pm i\omega) - i\kappa\beta\tau e^{-i\beta\delta}. \tag{8}$$

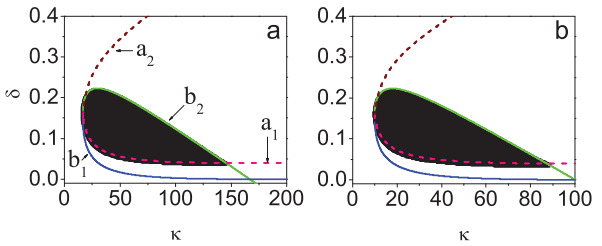

Fig. 5. The amplitude death island of the self-feedback coupled Stuart-Landau oscillator on the (κ, δ) space for $\tau = 0.006$ (a) and $\tau = 0.01$ (b). The solid lines come from analyses, they show good agreement with the numerical results (black points) in both the subfigures. (For interpretation of the references to color in this figure, the reader is referred to the web version of this article).

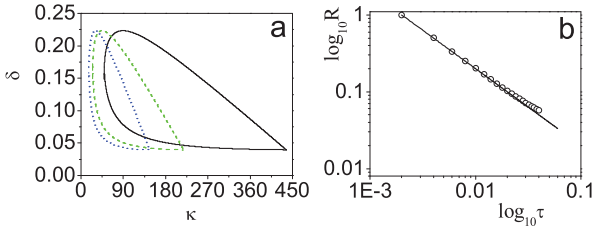

Fig. 6. (a) The amplitude death islands on the (κ, δ) space for $\tau = 0.002, 0.004$ and 0.006. The amplitude death island expands along the horizontal direction. (b) The normalized scaling factor R vs $.\tau$, with the data numerically computed (hollow points) and the fit (solid line) $R = \gamma\tau^{\mu}$, $\mu = -1.0, \gamma = 0.002$.

We have

$$\begin{aligned} \kappa\beta\tau\sin(\beta\tau) &= 1, \\ \kappa\beta\tau\cos(\beta\tau) &= -\beta \mp \omega. \end{aligned} \tag{9}$$

Further, we get

$$(\kappa\beta\tau)^2 = 1 + (\beta \pm \omega)^2, \tag{10}$$

we obtain

$$\beta_{1,2} = \frac{\omega \pm \sqrt{(\kappa\tau\omega)^2 + (\kappa\tau)^2 - 1}}{1 - (\kappa\tau)^2}. \tag{11}$$

After some algebraic manipulations, we further arrive at the following two equations:

$$\begin{aligned} \delta_{a_1,a_2}(\kappa) &= \frac{\pi - \sin^{-1}\left(\frac{1}{\kappa\tau\beta_{1,2}}\right)}{\beta_{1,2}}, \\ \delta_{b_1,b_2}(\kappa) &= \frac{\sin^{-1}\left(\frac{1}{\kappa\tau\beta_{1,2}}\right)}{\beta_{1,2}}. \end{aligned} \tag{12}$$

As an illustrated example, Fig. 5 shows the stable regions of amplitude death in the parameter plane of (κ, δ) for $\tau = 0.006, 0.01$, respectively. $\omega = 10$. All of the critical curves for different $\delta_{a_i,b_i}, i = 1, 2$ are shown in this figure. Totally, four critical curves determined by Eq. (12) are included and indicted by different colors and arrows. However, one can observe the curves δ_{a_2} and δ_{b_1} do not contribute to the region of amplitude death. The amplitude death domain, which is predicted by the critical curves δ_{a_1} and δ_{b_2}, has been well confirmed by direct numerical simulations (solid circles) of the self-feedback system (Eq. (3)).

We also explore the effect of τ on the size for region of amplitude death. Fig. 6(a) shows the region of amplitude death on the (κ, δ) plane with $\tau = 0.002, 0.004$, and 0.006, respectively. Interestingly, from Fig. 6(a), we find that the size of amplitude death island monotonically decreases with decreasing of τ. To quantify this size phenomenon, we introduce a normalized scaling factor $R = \frac{S_\tau}{S_{max}}$, where $S_\tau = \int_{\delta_{a_1} \le \delta_{b_2}} (\delta_{a_1} - \delta_{b_2}) d_\kappa$ denotes the area of death island for τ, and S_{max} for the maximal size. The value of R is numerically calculated and shown in Fig. 6(b). The hollow circles represent the numerical results. We find that R monotonically increases as propagation delay τ decreases before the propagation delay induces amplitude death ($\tau < 0.079$). This behavior is well characterized by the power law scaling,

$$R = \gamma\tau^{\mu}, \tag{13}$$

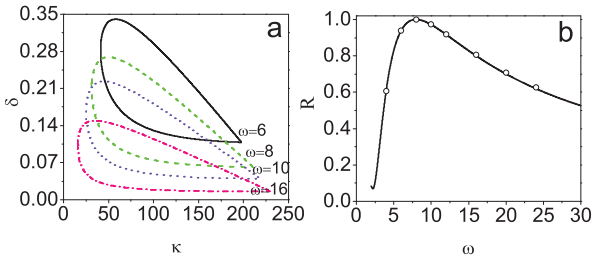

Fig. 7. (a) The amplitude death islands for $\omega = 6, 8, 10$ and 16, respectively. (b) The normalized scaling factor R vs. ω. The solid line which fits with the numerical results (open circles) well comes from analyses.

where $\mu = -1.0, \gamma = 0.002$. The power law relation can be clearly seen from a perfect log–log fit shown in Fig. 6(b). The power law function ($R = \gamma\tau^{\mu}$) is universal, as several other frequency parameters(e.g., $\omega = 5, 10, 15,$ or 20) have been systematically tested and all qualitative results have been found unchanged.

Eq. (12) shows that the frequency ω is involved in the amplitude death critical curves. Thus the size of the amplitude death region definitely depends on the value of ω. Fig. 7(a) displays several amplitude death islands for different values of $\omega = 6,$ 8, 10, and 16, respectively. $\tau = 0.004$ is fixed. The amplitude death region nonmonotonically depends on the frequency ω. This nonmonotonic dependence is shown clearly in Fig. 7(b) which shows R as a function of the frequency ω. There exists an optimal frequency ω such that the size of the amplitude death region becomes maximal. This phenomenon is totally different from the dependence on frequency for size of region which the propagation delay induces amplitude death.

4. The chaotic Rössler system

In order to further understand the effect of the process delay on dynamical behaviors in the nonlinear oscillators, we will analyze the self-feedback chaotic Rössler system [59], and the equations can be written as

$$\dot{x} = -y - z + \kappa(x(t-\delta-\tau) - x(t-\delta)), \tag{14a}$$

$$\dot{y} = x + ay + \kappa(y(t-\delta-\tau) - y(t-\delta)), \tag{14b}$$

$$\dot{z} = b + z(x-c)) + \kappa(z(t-\delta-\tau) - z(t-\delta)), \tag{14c}$$

where κ is the feedback gain, and the delays δ and τ physically account for the process time and propagation time, respectively. The parameters a, b, and c, are 0.15, 0.4, and 8.5, respectively. The oscillator is with phase coherent chaotic attractor under this parameter setting. The phase diagram of attractor resembles the limit cycle where the phase point always rotates around the origin on the plane (x, y), its topological property is rather simple.

Assuming the linear perturbation varies $e^{\lambda t}$, where λ is the eigenvalue, we obtain the following characteristic equation as the same as linear stability analysis of self-feedback coupled Stuart-Landau oscillator:

$$\lambda = \lambda_{0k} + \kappa(e^{-\lambda(\delta+\tau)} - e^{-\lambda\delta}), \tag{15}$$

where $\lambda_{0k} = 0.073 \pm i0.9973,\ -8.4575$ $(k = 1, 2, 3)$ are the eigenvalues of the unperturbed oscillator at the unstable fixed point, respectively. Some critical curves are obtained with the similar procedure in Section 3 for $\delta = 0$,

$$\begin{aligned}
\tau_a &= \frac{2m\pi + \cos^{-1}\left(\frac{\kappa-\lambda_{01}^R}{\kappa}\right)}{\lambda_{01}^I - \kappa\sqrt{1-\left(\frac{\kappa-\lambda_{01}^R}{\kappa}\right)^2}}, \\
\tau_b &= \frac{2(m+1)\pi - \cos^{-1}\left(\frac{\kappa-\lambda_{01}^R}{\kappa}\right)}{\lambda_{01}^I + \kappa\sqrt{1-\left(\frac{\kappa-\lambda_{01}^R}{\kappa}\right)^2}},
\end{aligned} \tag{16}$$

where m $(m = 0, 1, 2, ..., \infty)$ stands for the number of death islands, λ_{01}^R and λ_{01}^I are the real and imaginary part of λ_{01}, respectively. These critical curves are similar with the result in paper [27].

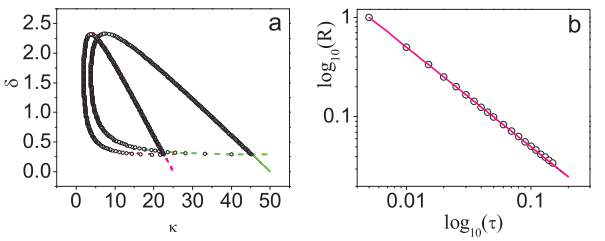

Fig. 8. (a) The amplitude death islands of the self-feedback chaotic Rössler system for $\tau = 0.02$ and $\tau = 0.04$. (b) The normalized scaling factor R vs. τ, The data for the numerical simulation (scatter points) fit well with analytical result (solid line).

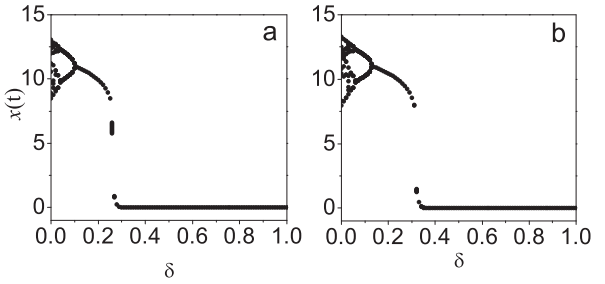

Fig. 9. (a) and (b) Bifurcation diagrams obtained by plotting the local maxima of $x(t)$ in Eq. (11). With increasing the process delay δ, the system experiences a reverse period-doubling bifurcation from chaos to one cycle.

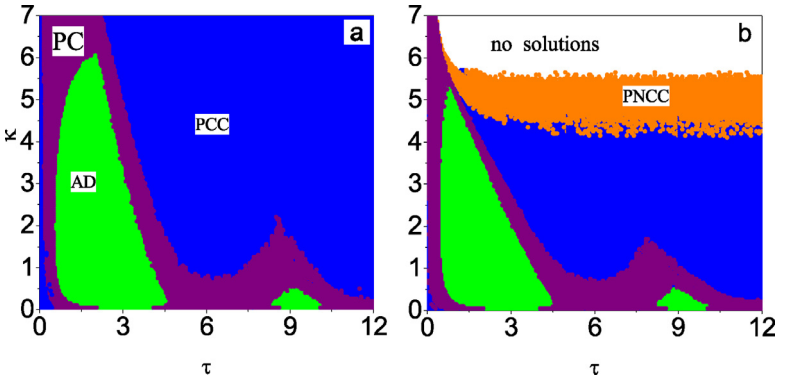

Fig. 10. (a) and (b) Phase diagram on the (τ, κ) plane for different dynamic regions of the self-feedback chaotic Rössler system for $\delta = 0.04$ and 0.06. The parameter space is separated into four regions, phase coherent chaotic state (PCC), phase noncoherent chaotic state (PNCC), periodic state (PS), and amplitude death (AD).

For $\delta \neq 0$, the approximate critical curves can also be gotten under the condition $\tau \ll \delta$,

$$\delta_{a_1}(\kappa) = \frac{\pi - \sin^{-1}\left(\frac{\lambda_{01}^R}{\kappa\tau\beta_1}\right)}{\beta_1},$$
$$\delta_{b_2}(\kappa) = \frac{\sin^{-1}\left(\frac{\lambda_{01}^R}{\kappa\tau\beta_2}\right)}{\beta_2}, \tag{17}$$

where $\beta_{1,2} = \frac{\lambda_{01}^I \pm \sqrt{(\kappa\tau\lambda_{01}^I)^2 + ((\kappa\tau)^2 - 1)(\lambda_{01}^R)^2}}{1-(\kappa\tau)^2}$. The critical boundary lines which do not have contributions are not shown. The results with solid lines are presented in Fig. 8(a) for different τ; they show good agreement with the numerical results (solid dots) in all the subfigures. Comparing these subfigures, we find that the size of death island gets smaller as τ increases. To quantify the change of this size clearly, the normalized scaling factor $R = S_\tau / S_{max}$ is shown in Fig. 8(b), where $S_\tau = \int_{\delta_{a_1} \le \delta_{b_2}} (\delta_{a_1} - \delta_{b_2}) d_\kappa$, One can easily see a monotonic decrease relationship between the value of R and τ, which is also described by a power law function.

To show the detail dynamics, Fig. 9 plots the bifurcation diagrams of the self-feedback system (Eq. (11)) which shows that with increasing the process delay δ, the system undergoes a reverse period-doubling cascade from chaos to one cycle,

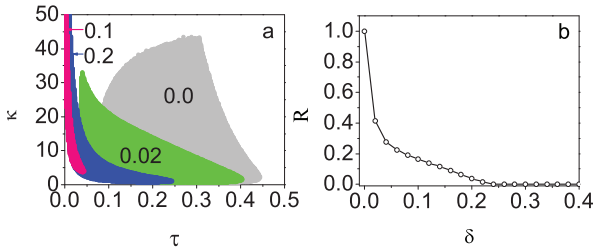

Fig. 11. (a) The amplitude death islands for $\delta = 0.0, 0.02, 0.1$ and 0.2, respectively. (b) The normalized scaling factor R vs. δ.

with a further increase in δ, the self-feedback system achieves amplitude death via a Hopf bifurcation. This observation clearly demonstrates that the process delay facilitates amplitude death in self-feedback chaotic oscillator.

We also numerically studied Eq. (11) in the parameter space of feedback gain and process delay time with different process delay. The results are shown in Fig. 10. The plane (τ, κ) is divided into four different dynamical regions: phase coherent chaotic state (PCC), phase noncoherent chaotic state (PNCC), periodic state (PS), and amplitude death (AD). Comparing two figures, one can observe that the phase noncoherent chaotic state merges if the process delay is sufficiently large, the process delay makes dynamics of system complex. The system have no solution for the sufficiently large process delays. To distinguish the phase coherent attractor and the phase noncoherent attractor, we used the method in paper [41]. To distinguish the chaotic state and period state, we use the method which is similar to the method in Section 2.

5. Conclusion and discussions

In conclusion, the role of process delay in feedback on the dynamical behavior of the nonlinear oscillators is investigated numerically and theoretically, and the rich dynamical phenomena are observed. For the delayed feedback FitzHugh–Nagumo neuronal model, the excite-spiking state, bursting state, unexcite-oscillate state, and multistable state are observed. For the periodic oscillator and chaotic system, the process delay can induce amplitude death before the transmission delay takes no effect in amplitude death, and the analytical death boundaries are also derived explicitly. Furthermore, we find that the transmission delay can reduce the area of the death island. The larger the value of transmission delay, the smaller the size of amplitude death island. The expansion well obeys a power law scaling, $R = \tau^{\gamma}$ $(\gamma < 0)$.

Below it is necessary to give some further discussions. In investigating the effect of process delay on amplitude death, the process delay is larger than the propagation delay. It is interesting to explore the opposite case $(\delta < \tau)$. Fig. 11(a) depicts the numerically obtained stable amplitude death for Stuart-Landau periodic oscillator with $\delta = 0.0$ 0.02 0.10.2, respectively. We can observe that the amplitude region shrinks monotonically as process delay is increased and vanishes if process delay surpasses the critical value. To quantify the change of this size clearly, the normalized scaling factor $R = S_{\tau}/S_{max}$ is shown in Figs. 11(b), From this plot, we can clearly see that R nonmonotonically depends on the value of process delay δ, indicating the process delay can eliminate the amplitude death. The similar results for process delay eliminating amplitude death can be gotten for the Rossler chaotic system. Our study can be a useful step to understand the effect of self-feedback loops and establish a method to control the stability of system by adjusting the process delay and transmission delay. All these results have been successfully extended to self-feedback dynamical systems with general nonlinearities. Finally we expect that the findings are of significance, and can provide a positive inducement for various experimental studies in future.

Acknowledgments

This work was supported partially by Natural Science Foundation of Zhejiang Province under Grant Nos. LY16A050001, the National Natural Science Foundation of China under Grant Nos. 11205103 and 179 11275129.

References

[1] Davidson E, Levin M. Gene regulatory networks. Proc Natl Acad Sci USA 2005;102:4935.
[2] Zhang H, Chen Y, Chen Y. Noise propagation in gene regulation networks involving interlinked positive and negative feedback loops. PLoS One 2015;7:e51840.
[3] Cabrera JL, Milton JG. On-off intermittency in a human balancing task. Phys Rev Lett 2002;89:158702.
[4] Bonan GB. Forests and climate change: forcings, feedbacks, and the climate benefits of forests. Science 2015;320:1444–9.
[5] Aronson BD, Johnson KA, Loros JJ, Dunlap JC. Negative feedback defining a circadian clock: autoregulation of the clock gene frequency. Science 1994;263:1578–84.
[6] Hardin PE, Hall JC, Rosbash M. Azimuthal anisotropy of velocity in the mantle lid beneath the basin and range province. Natue 1990;348:536–8.
[7] Lubke J, Markram H, Frotscher M, Sakmann B. Frequency and dendritic distribution of autapses established by layer 5 pyramidal neurons in the developing rat neocortex: comparison with synaptic innervation of adjacent neurons of the same class. J Neurosci 1996;16:3209–18.
[8] Van H, Der L, Glaser EM. Autapses in neocortex cerebri: synapses between a pyramidal cell' s axon and its own dendrites. Brain Res 1972;48(355):355–60.
[9] Bekkers JM. Neurophysiology: Are autapses prodigal synapses? Curr Biol 1998;8:R52–5.
[10] Flight MH. Axon degeneration: committing to a break up. Nat Rev Neurosci 2009;10:316–17.

[11] Bekkers JM. Synaptic transmission: functional autapses in the cortex. Curr Biol 2003;13:R433–5.
[12] Saada R, Miller N, Hurwitz I, Susswein AJ. Autaptic excitation elicits persistent activity and a plateau potential in a neuron of known behavioral function. Curr Biol 2009;19:479–84.
[13] Bacci A, Huguenard JR. Enhancement of spike-timing precision by autaptic transmission in neocortical inhibitory interneuronsoriginal research. Neuron 2006;49:119–30.
[14] Bacci A, Huguenard JR, Prince DA. Functional autaptic neurotransmission in fast-spiking interneurons: a novel form of feedback inhibition in the neocortex. J Neurosci 2003;23:859–66.
[15] Qin H, Ma J, Wang C, Wu Y. Autapse-induced spiral wave in network of neurons under noise. PLoS One 2014;9:e100849.
[16] Wu Y, Gong Y, Wang Q. Autaptic activity-induced synchronization transitions in Newman–Watts network of Hodgkin–Huxley neurons. Chaos 2015;2:043113.
[17] Wang Q, Gonga Y, Wu Y. Autaptic self-feedback-induced synchronization transitions in Newman–Watts neuronal network with time delays. Phys J B 2015;88:103.
[18] Wang H, Wang L, Chen Y, Chen Y. Effect of autaptic activity on the response of a Hodgkin–Huxley neuron. Chaos 2014;24:033122.
[19] Li Y, Schmid G, Haggi P, Schimansky-Geier L. Spontaneous spiking in an autaptic Hodgkin–Huxley setup. Phy Rev E 2010;82:061907.
[20] Hashemi M, Valizadeh A, Azizi Y. Effect of duration of synaptic activity on spike rate of a Hodgkin–Huxley neuron with delayed feedback. Phy Rev E 2012;85:021917.
[21] Zeng C, Zeng C, Gong A, Nie L. Effect of time delay in Fitzhugh–Nagumo neural model with correlations between multiplicative and additive noises. Physica A 2010;389:5117–27.
[22] Prager T, Lerch HP, Schimansky-Geier L, Scholl E. Increase of coherence in excitable systems by delayed feedback. J Phys A: Math Theor 2007;40:11045.
[23] Schuster HG. Handbook of chaos control. Weinheim: Wiley-VCH; 1999.
[24] Boccaletti S, Grebogi C, Lai YC, Mancini H, Maza D. The control of chaos: theory and applications. Phys Rep 2000;329:103–97.
[25] Gauthier D, Hall GM, Olivier RA, Dixon-Tulloch EG, Wolf PD, Bahar S. Progress toward controlling in vivo fibrillating sheep atria using a nonlinear-dynamics-based closed-loop feedback method. Chaos 2003;12:952.
[26] Hoel P, Schol E. Stabilizing unstable periodic orbits in the lorenz equations using time-delayed feedback control. Phys Rev E 2007;76:056214.
[27] Ryu JW, Kye WH, Lee SY, Kim MW, Choi M, Rim S, et al. Effects of time-delayed feedback on chaotic oscillators. Phys Rev E 2004;70:036220.
[28] Ramana Reddy DV, Sen A, Johnston GL. Dynamics of a limit cycle oscillator under time delayed linear and nonlinear feedbacks. Physica D 2000;144:335–57.
[29] Zou W, Senthilkumar DV, Nagao R, Kiss IZ, Tang Y, Koseska A, et al. Restoration of rhythmicity in diffusively coupled dynamical networks. Nat Commun 2015;6:7709.
[30] Ahlborn A, Parlitz U. Control and synchronization of spatiotemporal chaos. Phys Rev E 2008;77:016201.
[31] Gaudreault M, Drolet F, Vinals J. Bifurcation threshold of the delayed van der pol oscillator under stochastic modulation. Phys Rev E 2012;85:056214.
[32] Yanchuk S, Wolfrum M, Hoel P, Schol E. Control of unstable steady states by long delay feedback. Phys Rev E 2006;74:026201.
[33] Bielawski S, Derozier D, Glorieux P. Controlling unstable periodic orbits by a delayed continuous feedback. Phys Rev E 1994;49:R971.
[34] Gauthier DJ, Sukow DW, Concannon HM, Socolar JES. Stabilizing unstable periodic orbits in a fast diode resonator using continuous time-delay autosynchronization. Phys Rev E 1994;50:2343.
[35] Lekebusch A, Foster A, Schneider FW. Chaos control by electric current in an enzymatic reaction. Int J Neural Syst 1996;07:393.
[36] Fukuyama T, Shirahama H, Kawai Y. Dynamical control of the chaotic state of the current-driven ion acoustic instability in a laboratory plasma using delayed feedback. Phys Plasmas 2002;9:4525.
[37] Pyragas K. Continuous control of chaos by self-controlling feedback. Phys Lett A 1992;170:421–8.
[38] Schuster HG, Wagner P. Mutual entrainment of two limit cycle oscillators with time delayed coupling. Prog Theor Phys 1989;81:939–45.
[39] Strogatz SH. Nonlinear dynamics: death by delay. Nature 1998;394:316–17.
[40] Yao CG, Zou W, Zhao Q. The study of amplitude death in globally delay-coupled nonidentical systems based on order parameter expansion. Chaos 2012;22:023149.
[41] Yao CG, Zhao Q, Liu WQ, Yu J. Collective dynamics induced by diversity taken from two-point distribution in globally coupled chaotic oscillators. Nonlinear Dyn 2014;75:17–26.
[42] Prasad A. Amplitude death in coupled chaotic oscillators. Phys Rev E 2005;72:056204.
[43] Zou W, Yao CG, Zhan M. Eliminating delay-induced oscillation death by gradient coupling. Phys Rev E 2010;82:056203.
[44] Konishi K, Kokame H, Hara N. Stabilization of a steady state in network oscillators by using diffusive connections with two long time delays. Phys Rev E 2010;81:016201.
[45] Zou W, Tang Y, Li LX, Kurths J. Oscillation death in asymmetrically delay-coupled oscillators. Phys Rev E 2014;85:046206.
[46] Zou W, Senthilkumar DV, Zhan M, Kurths J. Reviving oscillations in coupled nonlinear oscillators. Phys Rev Lett 2013;111:014101.
[47] Hunt D, Korniss G, Szymanski BK. Network synchronization in a noisy environment with time delays: fundamental limits and trade-offs. Phys Rev Lett 2010;105:068701.
[48] Hunt D, Korniss G, Szymanski BK. The impact of competing time delays in coupled stochastic systems. Phys Lett A 2011;375:880–5.
[49] Hod S. Analytic treatment of the network synchronization problem with time delays. Phys Rev Lett 2010;105:208701.
[50] Jensen AR. Clocking the mind: mental chronometry and individual differences. Amsterdam: Elsevier; 2006.
[51] Senthilkumar D.V., Suresh K., Chandrasekar V.K., Zou W., Dana S.K., Thamilmaran K., et al. Experimental demonstration of death and revival of oscillations in coupled nonlinear oscillators. (Submitted for publication).
[52] Keener J, Snyder J. Mathematical physiology. New York: Springer; 1998.
[53] Fitzhugh R. Motion picture of nerve impulse propagation using computer animation. J Appl Physiol 1968;25:628–30.
[54] Tessone CJ, Mirasso CR, Toral R, Gunton JD. Diversity-induced resonance. Phys Rev Lett 2006;97:194101.
[55] FitzHugh R. Impulses and physiological states in theoretical models of nerve membrane. Biophys J 1961;1:445–66.
[56] Deng B, Wang J, Wei XL. Effect of chemical synapse on vibrational resonance in coupled neurons. Chaos 2009;19:013117.
[57] Pikovsky AS, Kurths J. Coherence resonance in a noise-driven excitable system. Phys Rev E 1997;78:775.
[58] Kuramoto Y. Chemical oscillations, waves, and turbulence. New York: Springer; 1984.
[59] Rossler OE. An equation for continuous chaos. Phys Lett A 1976;57:397–8.